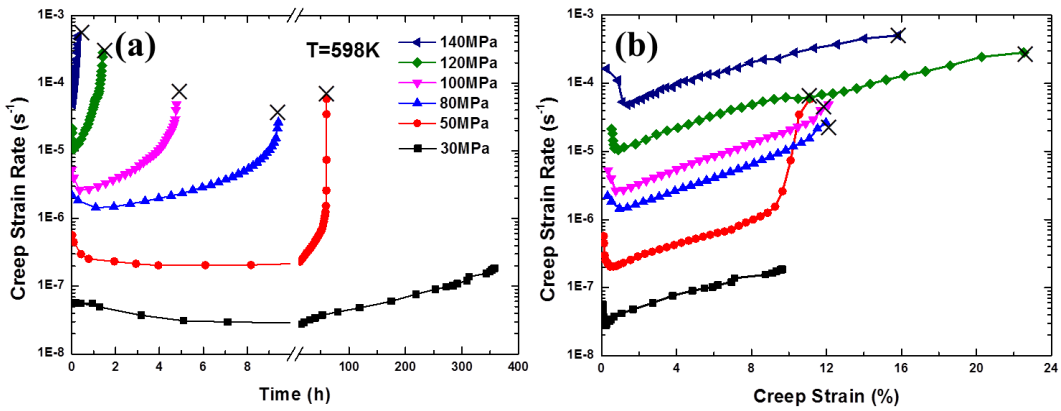

Fig. 1. Creep rate curves of the WGZ1152-T6 at T=598K: (a) creep strain rate versus time; (b) creep strain rate versus creep strain. Note that the specimens which were creep tested to failure were indicated with "X".

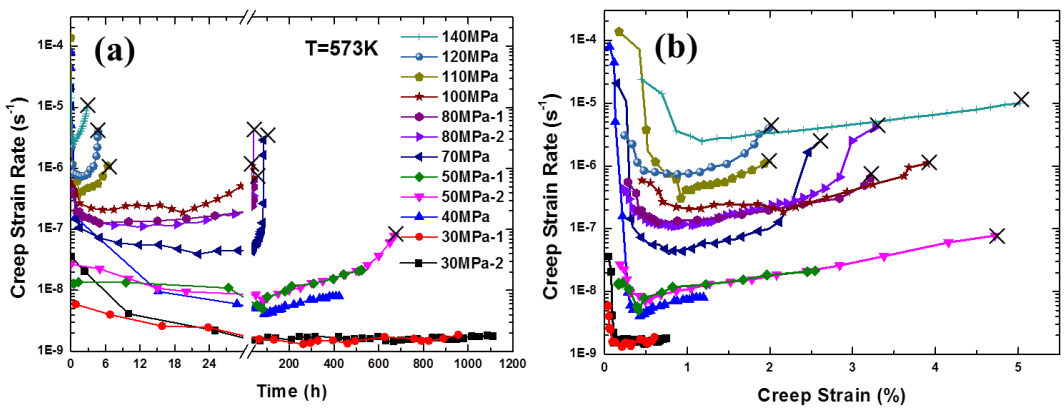

Fig. 2. Creep rate curves of the WGZ1152-T6 at T=573K: (a) creep strain rate versus time; (b) creep strain rate versus creep strain. Note that the specimens which were creep tested to failure were indicated with "X".

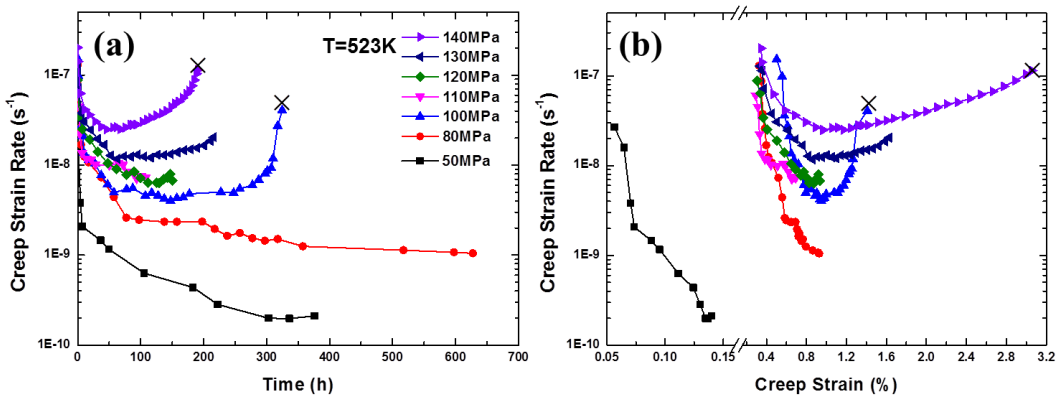

Fig. 3. Creep rate curves of the WGZ1152-T6 at T=523K: (a) creep strain rate versus time; (b) creep strain rate versus creep strain. Note that the specimens which were creep tested to failure were indicated with "X".

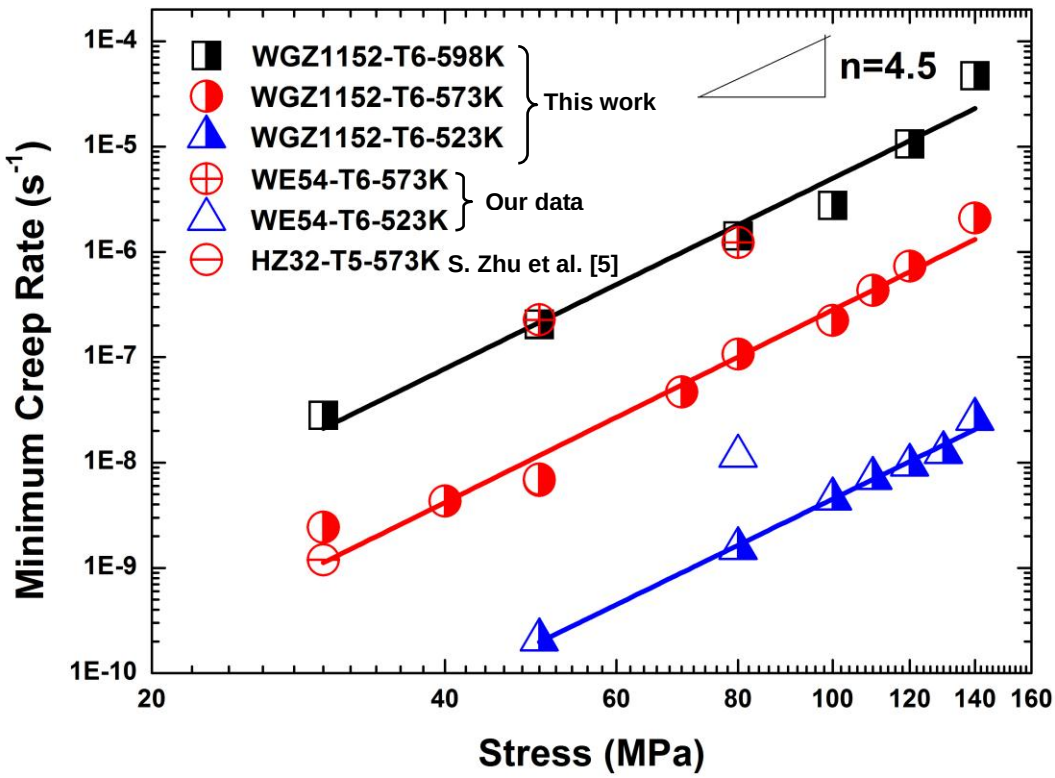

Fig. 4. Log-Log plot of the stress dependence on the minimum creep rate at T=523-598K. Note that the data of WE54-T6 and HZ32[5]-T5 were also presented for comparison.

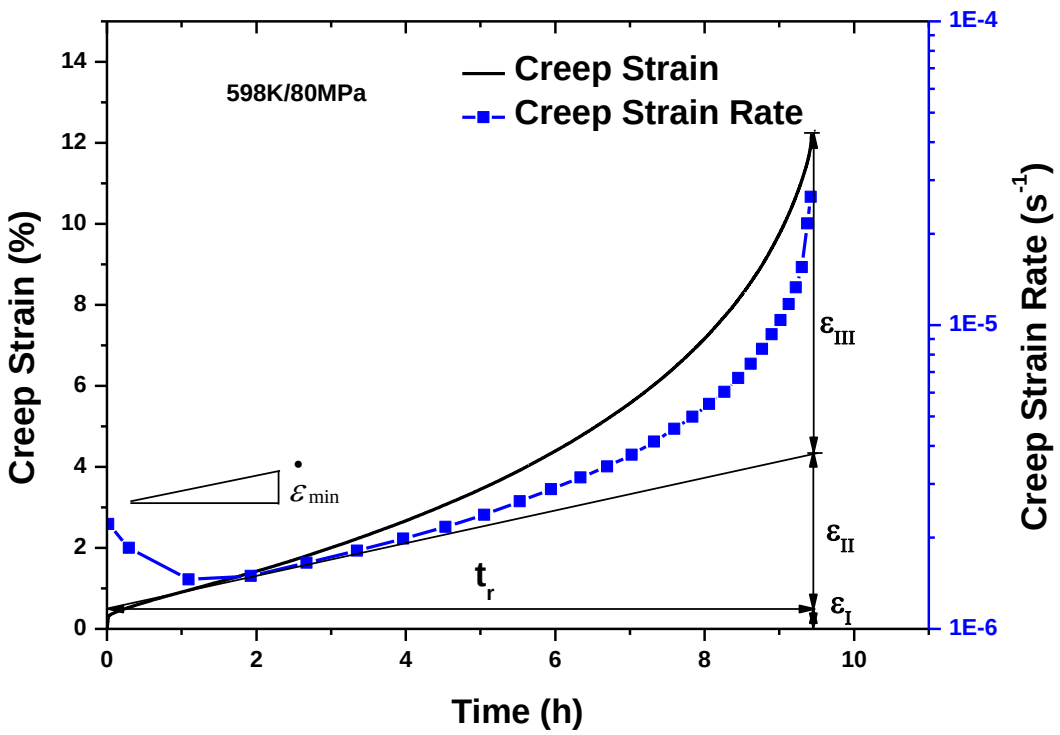

Fig. 5. Representative creep curve of the WGZ1152-T6 at T=598K and σ=80MPa showing the primary stage strain ε_I, the secondary stage strain ε_{II} and the tertiary stage strain ε_{III}, along with the creep strain rate as a function of time.

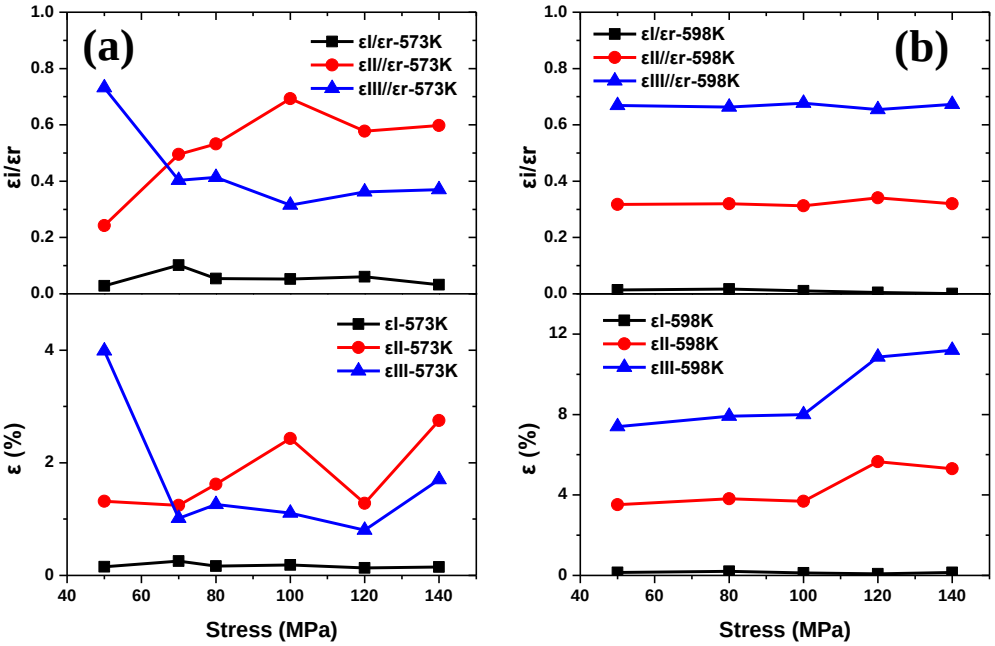

Fig. 6. Stress dependence of the primary stage strain ε_I, the secondary stage strain ε_{II}, the tertiary stage strain ε_{III} and the relative strain per creep stage $\varepsilon_i/\varepsilon_r$ (i = I, II, III), ε_r=total creep strain, at (a) 573K and (b) 598K. At 598K, the majority of the strain was archived in the tertiary creep stage.

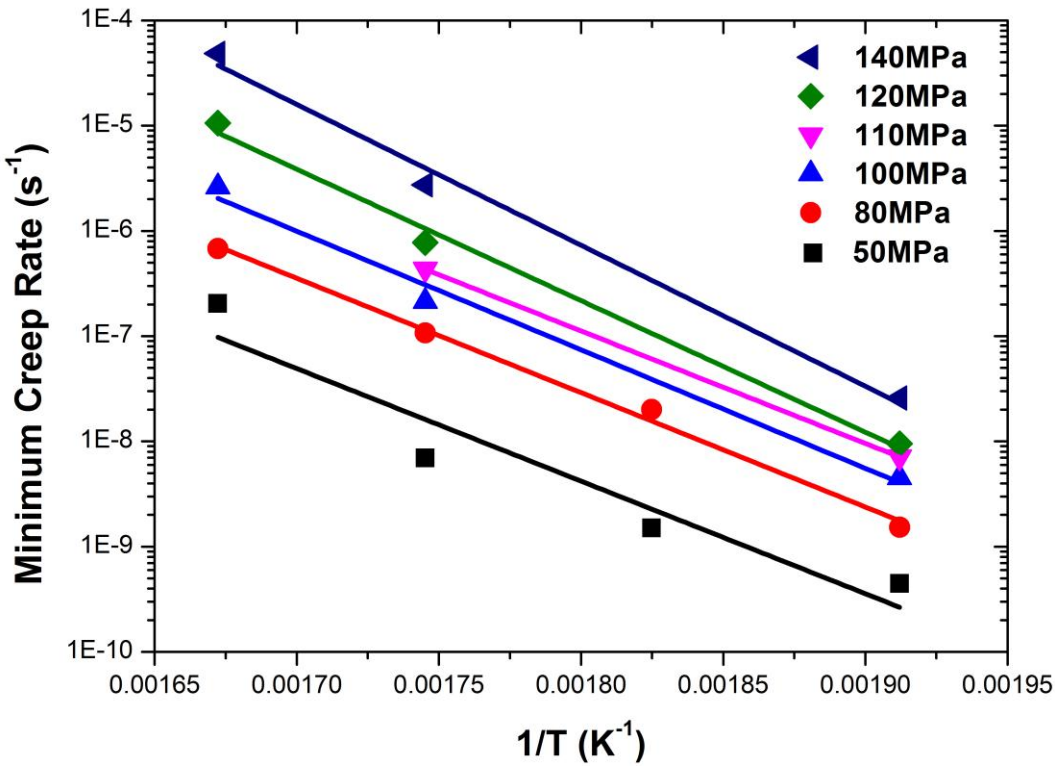

Fig. 7. The Arrhenius plot of the natural logarithm of minimum creep rate versus the reciprocal of temperature at stresses between 50MPa to 140MPa.

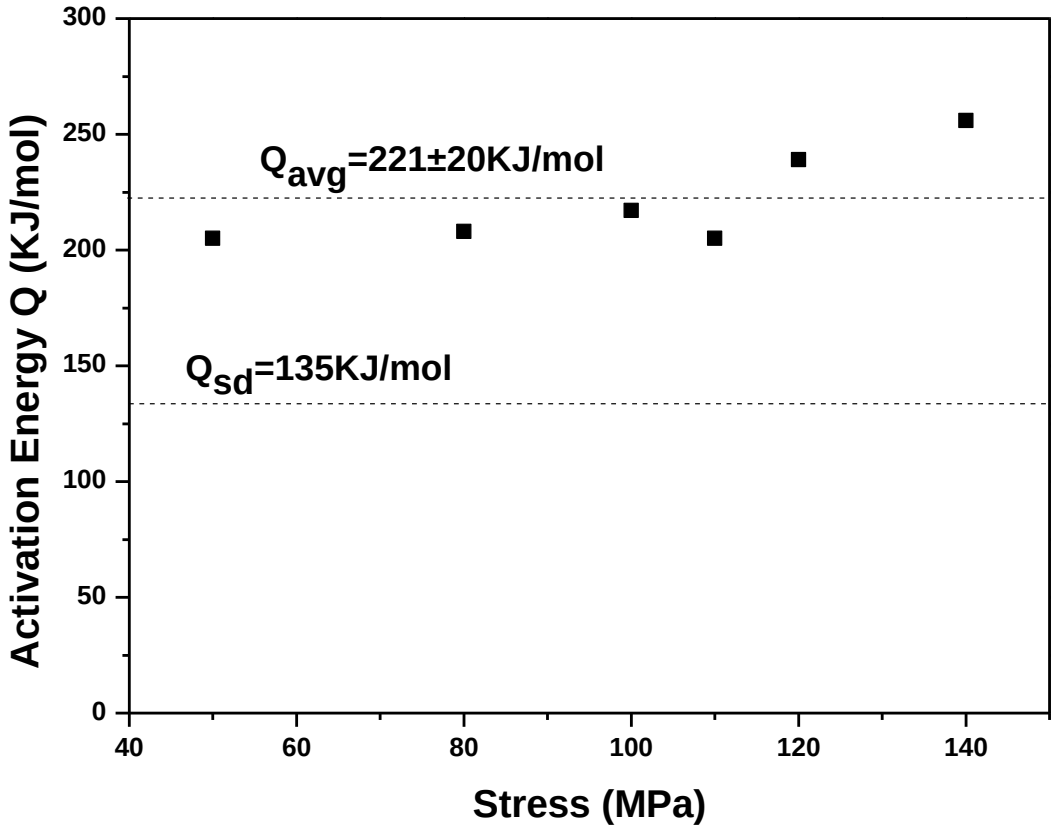

Fig. 8. Activation energy Q for creep versus stress.

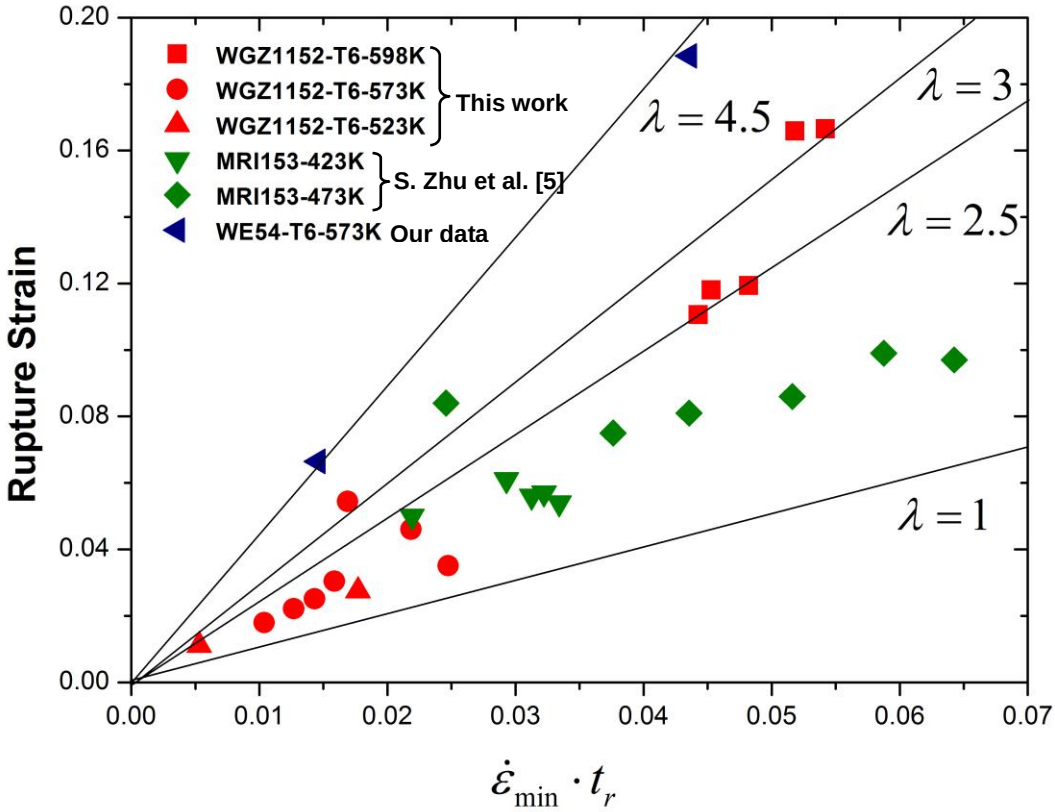

Fig. 9. Relationship between rupture strain ε_r and $\dot{\varepsilon}_{\min} \cdot t_r$, where t_r=rupture time, showing the creep damage tolerance parameter λ. Note that the data of MRI153[5] and WE54-T6 were also presented for comparison.

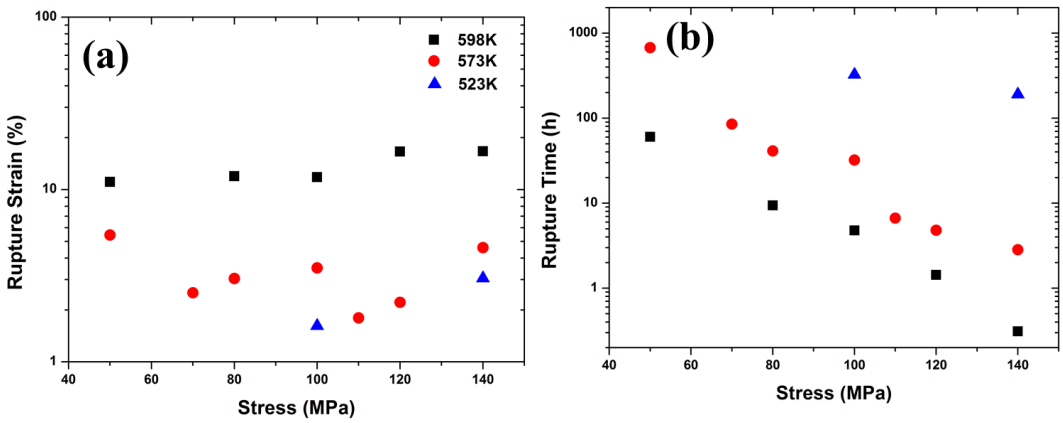

Fig. 10. The stress dependence on (a) creep rupture strain and (b) creep rupture time at T=523-598K.

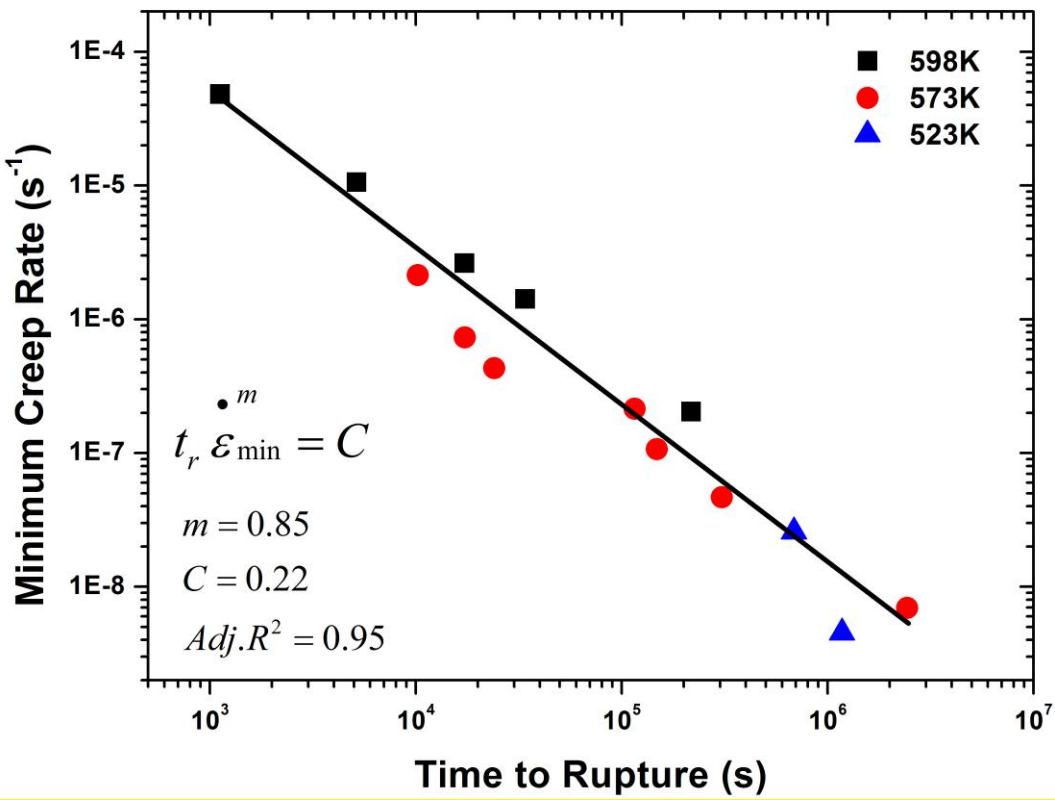

Fig. 11. Log-Log plot of minimum creep rate versus time-to-rupture at T=523-598K and stresses between 50MPa to 140MPa illustrating the Monkman-Grant relationship (MGR).

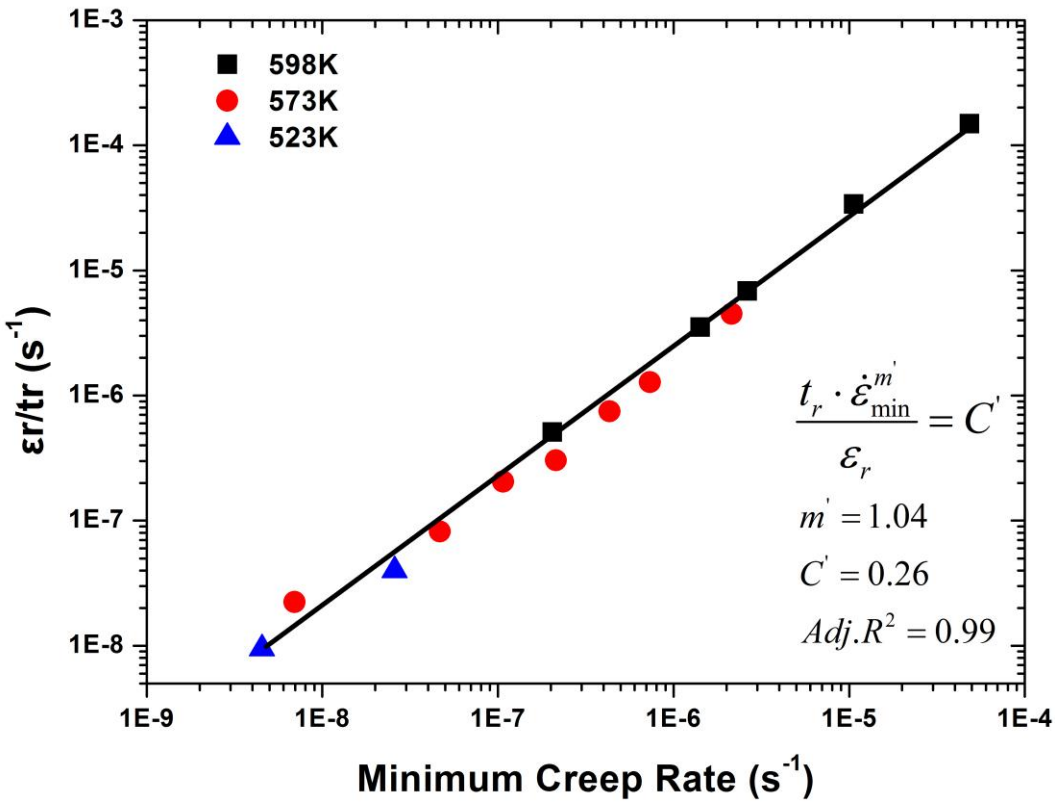

Fig. 12. Log-Log plot of ε_r/t_r versus minimum creep rate at T=523-598K and stresses between 50MPa to 140MPa illustrating the modified Monkman-Grant relationship (MMGR).

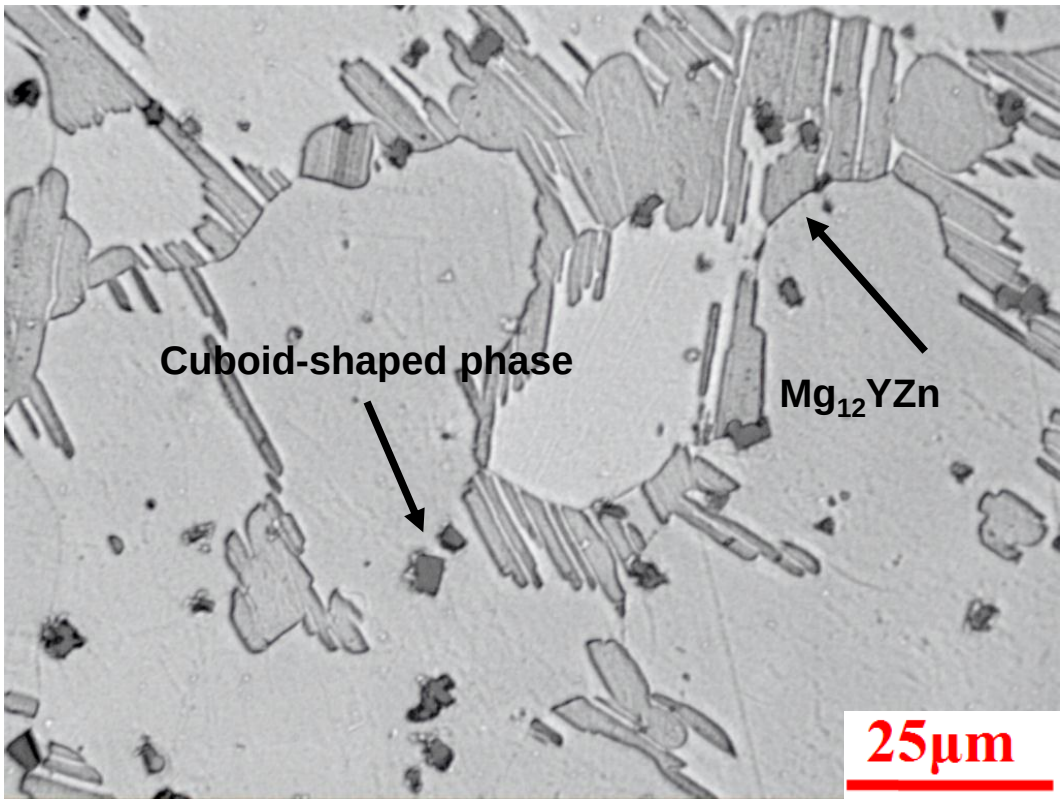

Fig. 13. Optical photomicrograph of the peak-aged WGZ1152-T6 microstructure.

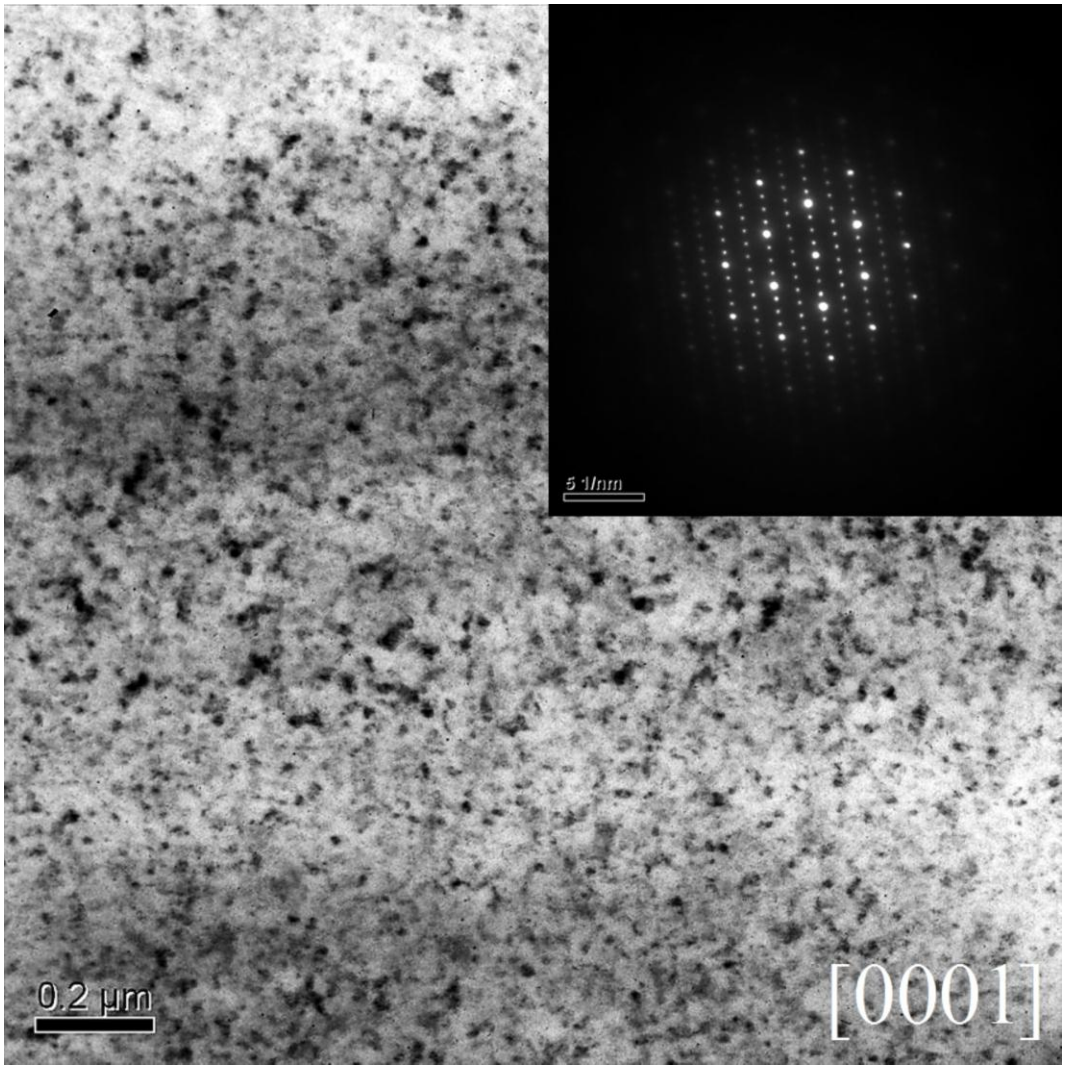

Fig. 14. TEM bright field image and SADP of the fine β′ precipitates in peak-aged WGZ1152-T6. The beam direction is approximately parallel to [0001] zone axis.

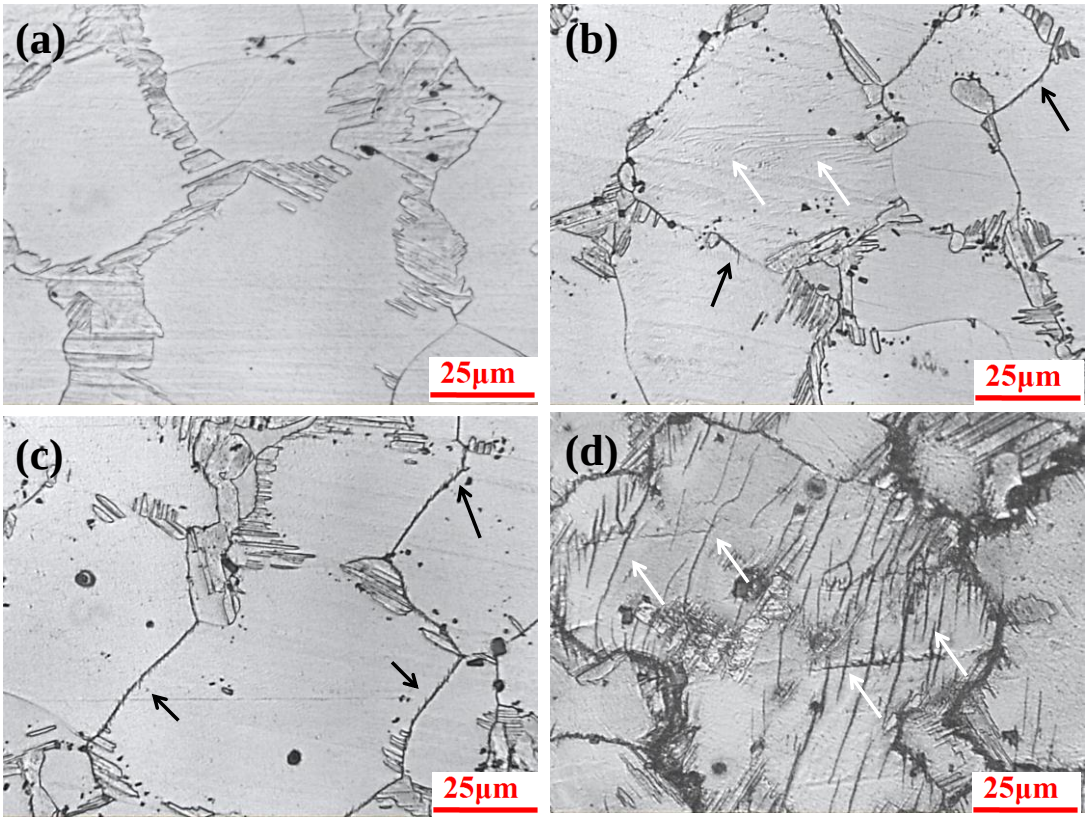

Fig. 15. Optical photomicrographs of the surface of specimens creep tested at T=598K and σ=50MPa illustrating microstructural evolution during creep exposure: (a) creep stage I (t=0.5h, ε=0.10%), (b) and (c) creep stage II (t=5h, ε=0.45%) and (d) creep stage III (t=50h, ε=6.2%). The tensile axis was horizontal.

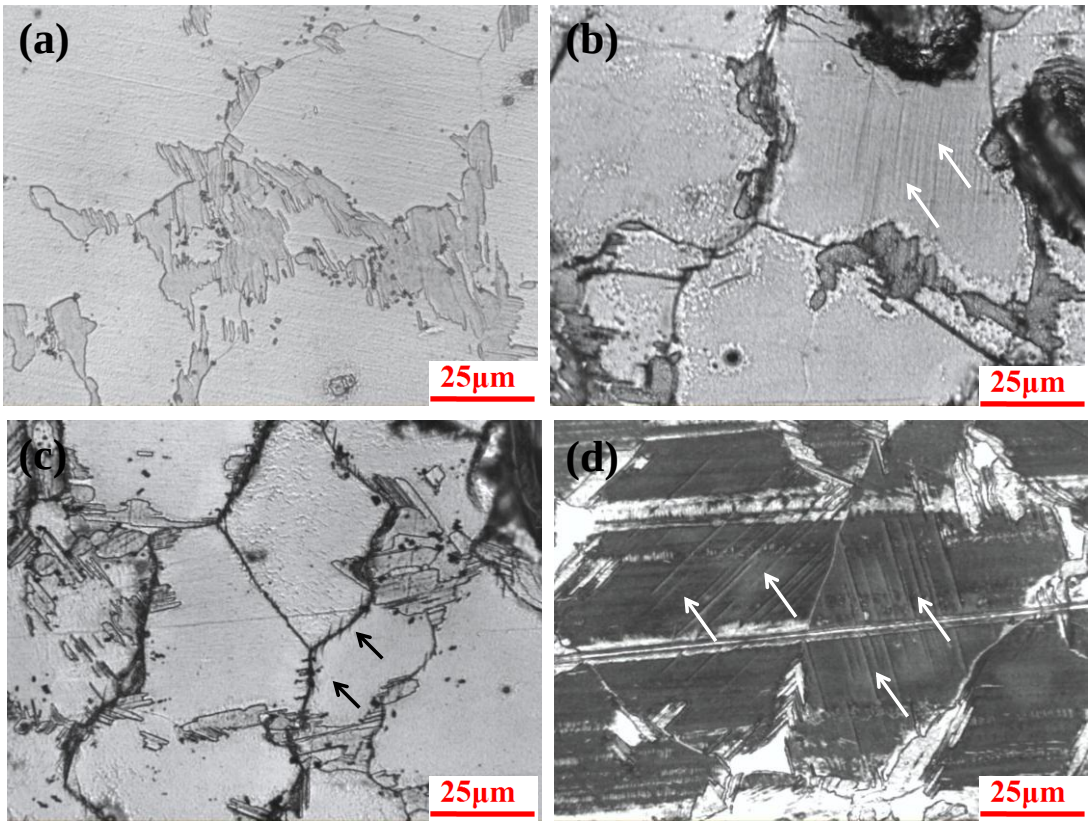

Fig. 16. Optical photomicrographs of the surface of specimens creep tested at T=573K and σ=50MPa [(a)-(c)] illustrating microstructural evolution during creep exposure: (a) creep stage I (t=5h, ε=0.05%), (b) and (c) creep stage II (t=90h, ε=0.42%). (d) Creep tested at T=523K and σ=50MPa, creep stage II (t=380h, ε=0.19%). The tensile axis was horizontal.

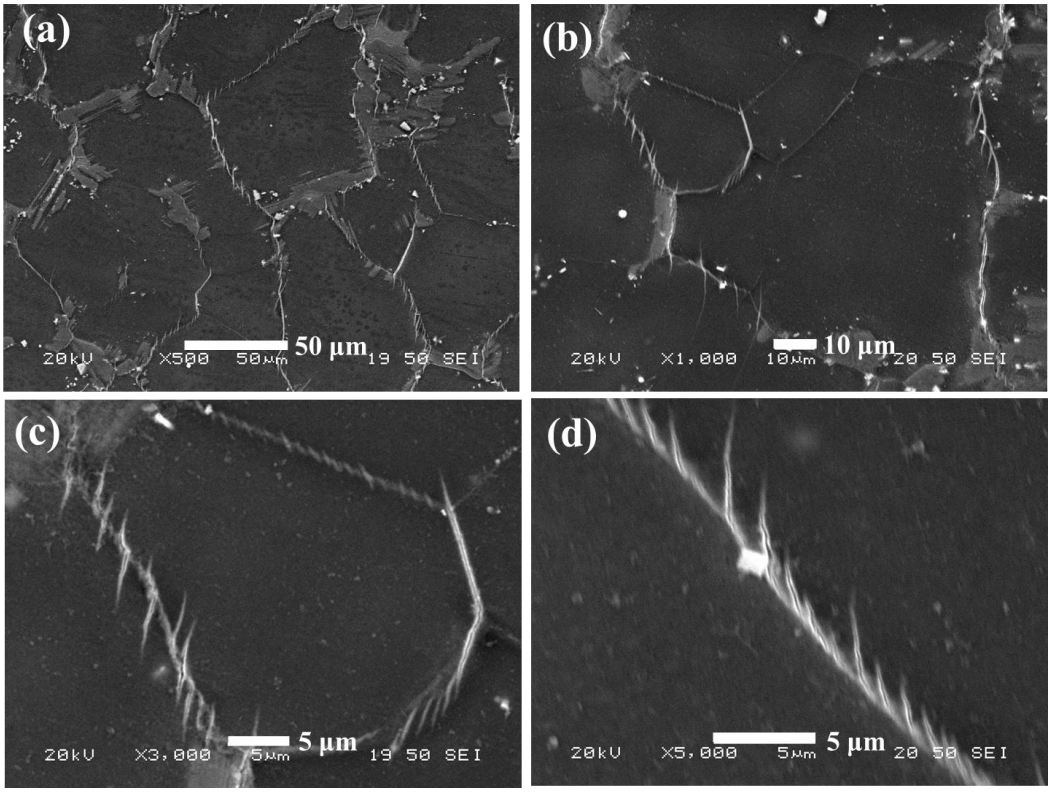

Fig. 17. Secondary electron SEM photomicrographs of the surface of a specimen creep tested to stage II (t=90h, ε=0.42%) at T=573K and σ=50MPa showing microcracks near grain boundaries. The tensile axis was horizontal.

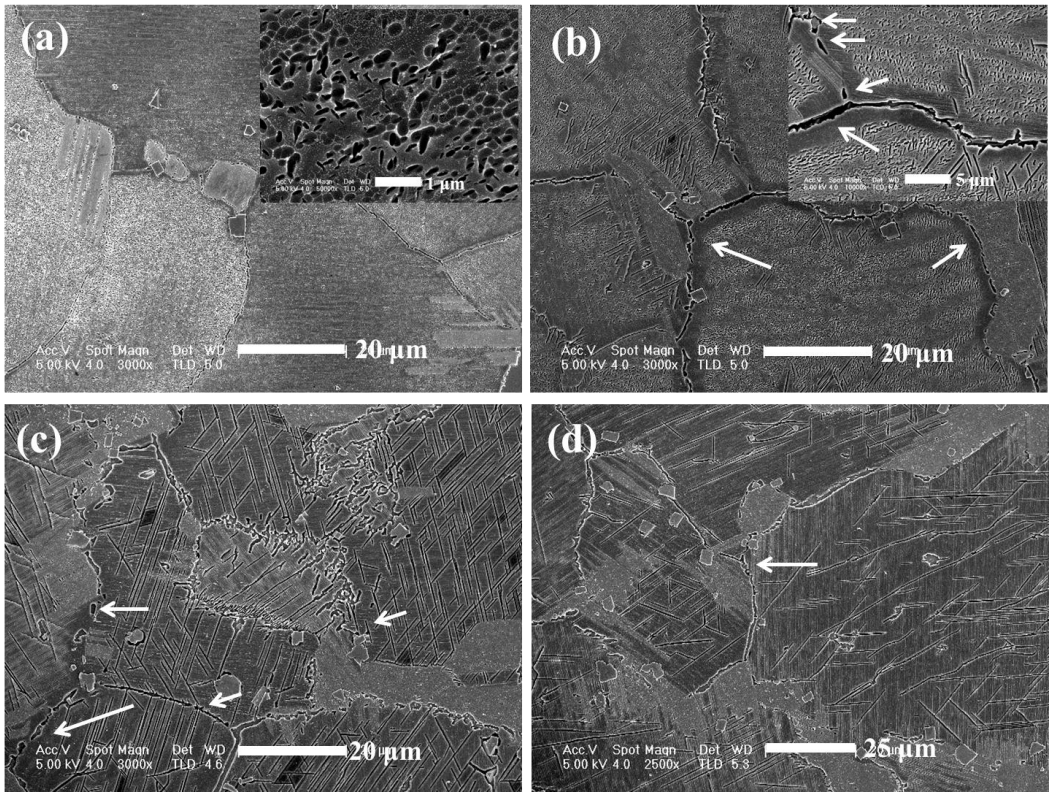

Fig. 18. Secondary electron SEM photomicrographs of creep tested specimens: (a) t=4.8h, ε=2.2% (T=573K and σ=120MPa), (b) t=85h, ε=2.5% (T=573K and σ=70MPa), (c) t=676h, ε=5.4% (T=573K and σ=50MPa) and (d) t=1114h, ε=1.2% (T=573K and σ=30MPa).

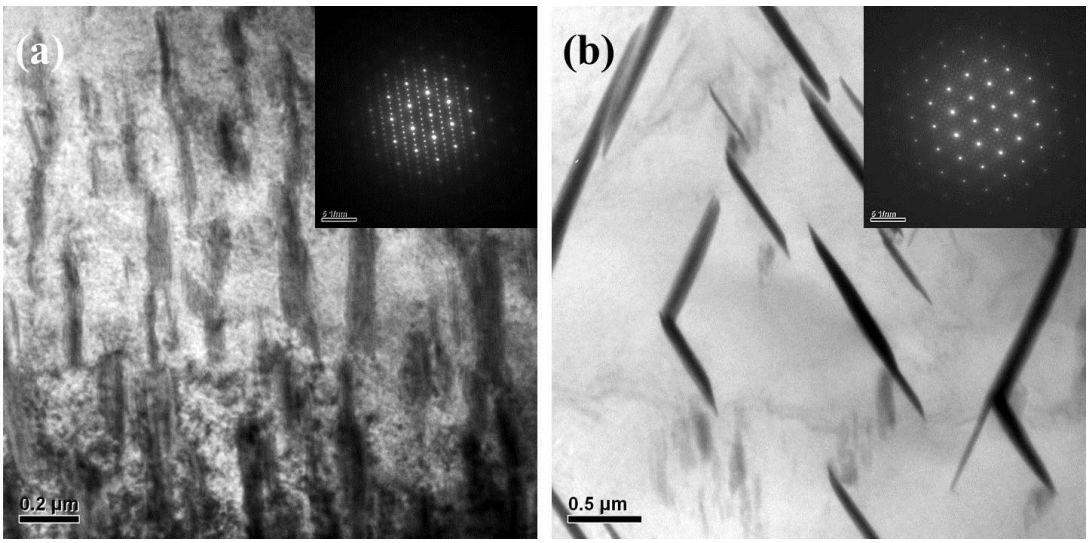

Fig. 19. TEM bright field images and SADPs of creep tested specimens with different creep time, showing (a) coarsed β′ precipitates, t=41h, ε=3.0% (T=573K and σ=80MPa) and (b) β precipitates, t=676h, ε=5.4% (T=573K and σ=50MPa). The beam direction was approximately parallel to [0001] zone axis.

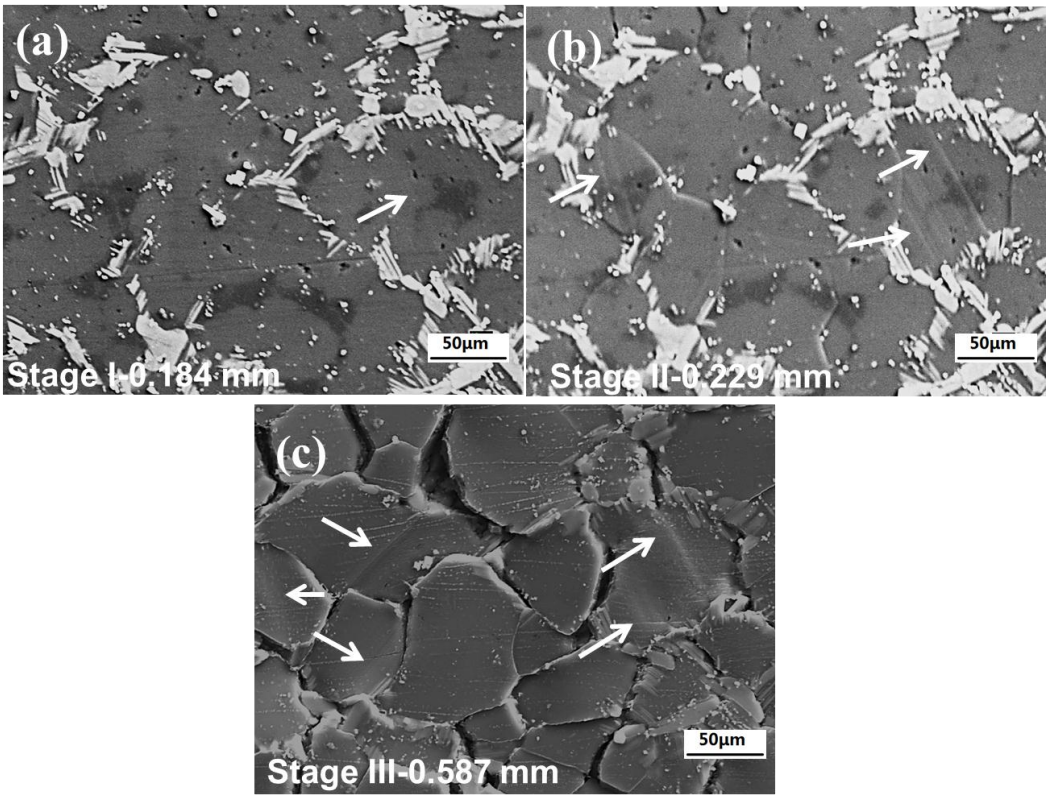

Fig. 20. Secondary electron SEM photomicrographs taken during an *in-situ* creep test at T=573K and σ=50MPa, where the number of surface slip traces (indicated with arrows) bands increased with increased creep time. The creep stages and displacements were indicated in the figures. The tensile axis was horizontal.

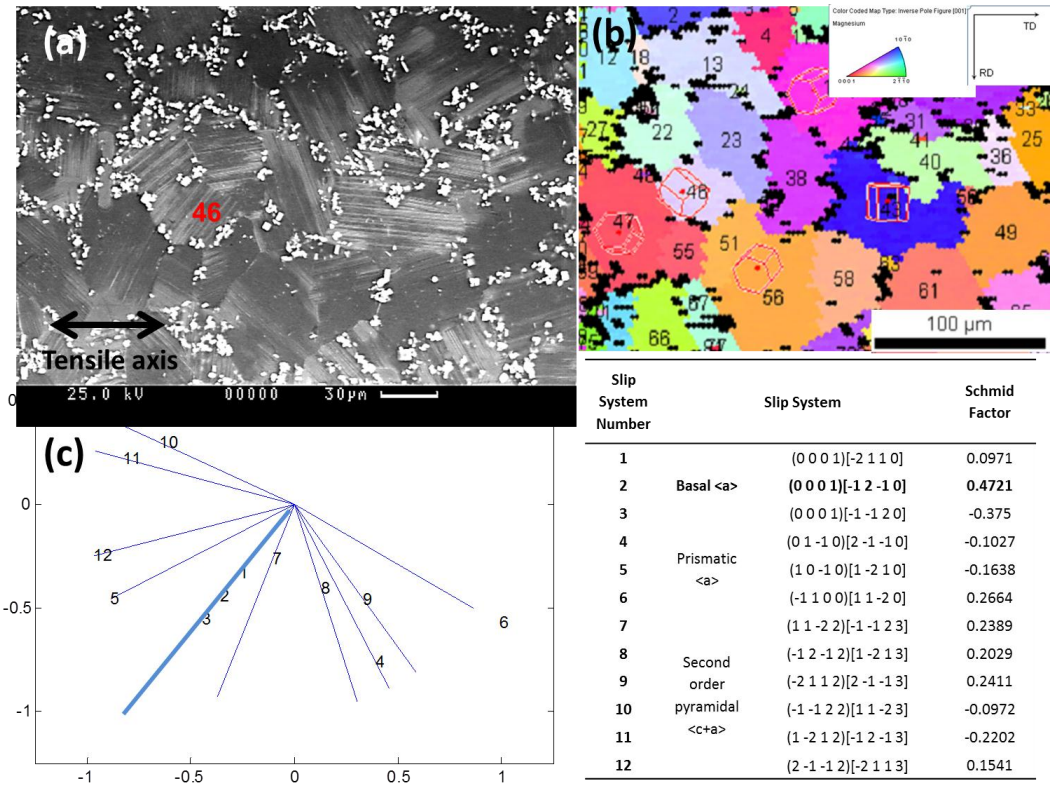

Slip System Number		Slip System	Schmid Factor
1		(0 0 0 1)[-2 1 1 0]	0.0971
2	**Basal <a>**	**(0 0 0 1)[-1 2 -1 0]**	**0.4721**
3		(0 0 0 1)[-1 -1 2 0]	-0.375
4	Prismatic <a>	(0 1 -1 0)[2 -1 -1 0]	-0.1027
5		(1 0 -1 0)[1 -2 1 0]	-0.1638
6		(-1 1 0 0)[1 1 -2 0]	0.2664
7		(1 1 -2 2)[-1 -1 2 3]	0.2389
8	Second order pyramidal <c+a>	(-1 2 -1 2)[1 -2 1 3]	0.2029
9		(-2 1 1 2)[2 -1 -1 3]	0.2411
10		(-1 -1 2 2)[1 1 -2 3]	-0.0972
11		(1 -2 1 2)[-1 2 -1 3]	-0.2202
12		(2 -1 -1 2)[-2 1 1 3]	0.1541

Fig. 21. Examples of the slip trace analysis performed to grain NO. 46 in (a), taken for the sample *in-situ* creep tested at T=573K and σ=50MPa. (a) the SE SEM photomicrograph, (b) EBSD orientation maps in ND, and (c) the slip system selection. Note that 2 was the selected system based on the match and this corresponds to the (0 0 0 1) plane and [-1 2 -1 0] direction. The Schmid factors for the slip systems are indicated on the right hand side.

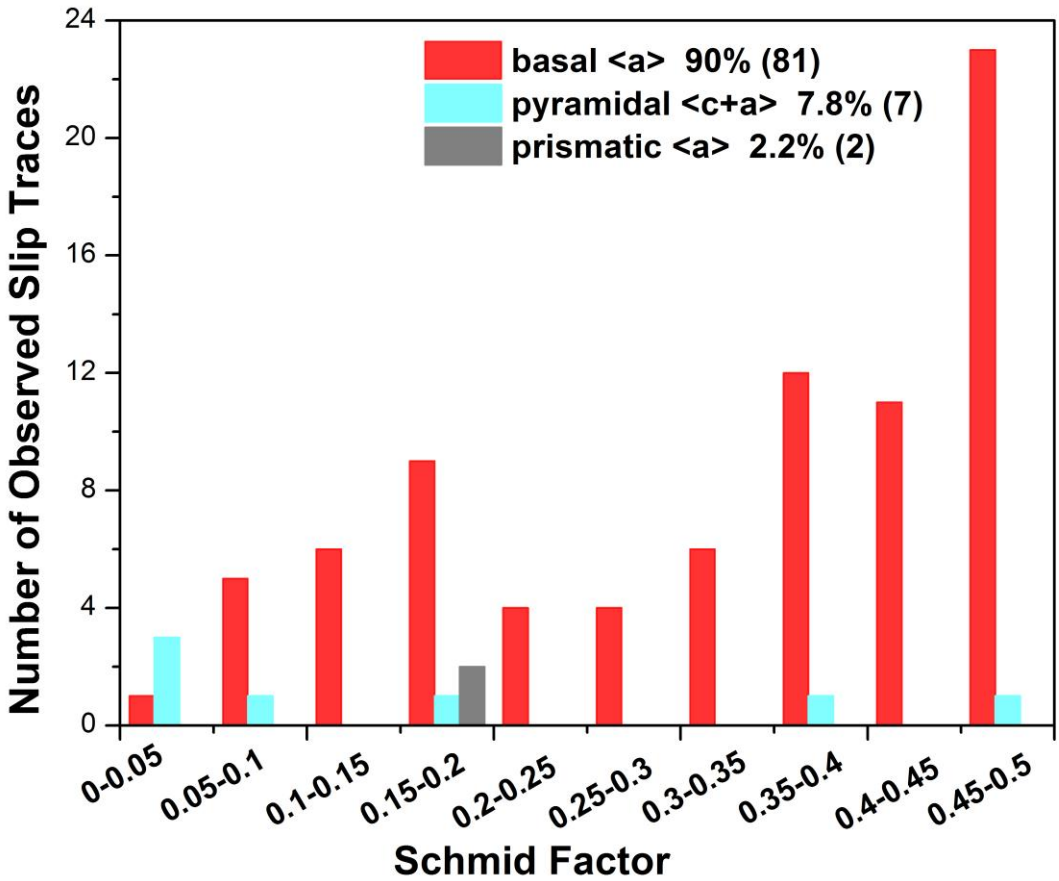

Fig. 22. The Schmid factor distributions and the number of identified slip systems for the sample *in-situ* creep tested at T=573K and σ=50MPa.

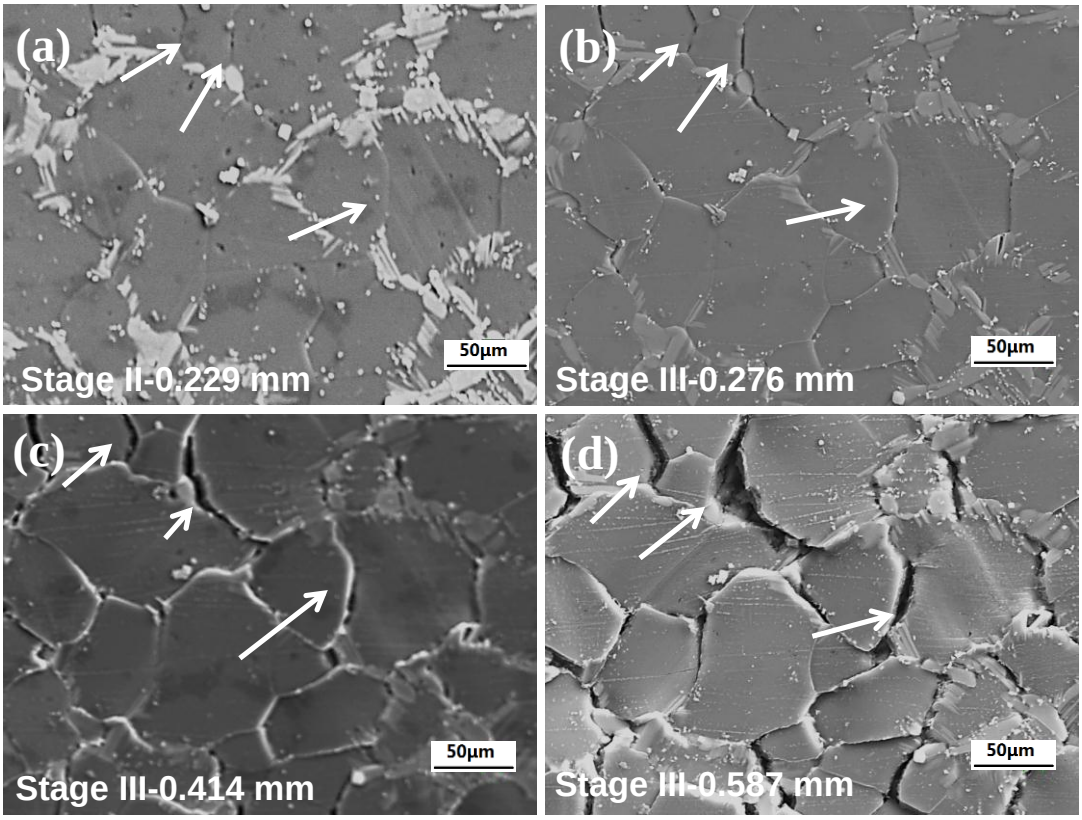

Fig. 23. Secondary electron SEM photomicrographs taken during an *in-situ* creep test at T=573K and σ=50MPa illustrating intergranular cracking initiation and propagation. The creep stages and displacements were indicated in the figures. The tensile axis was horizontal.

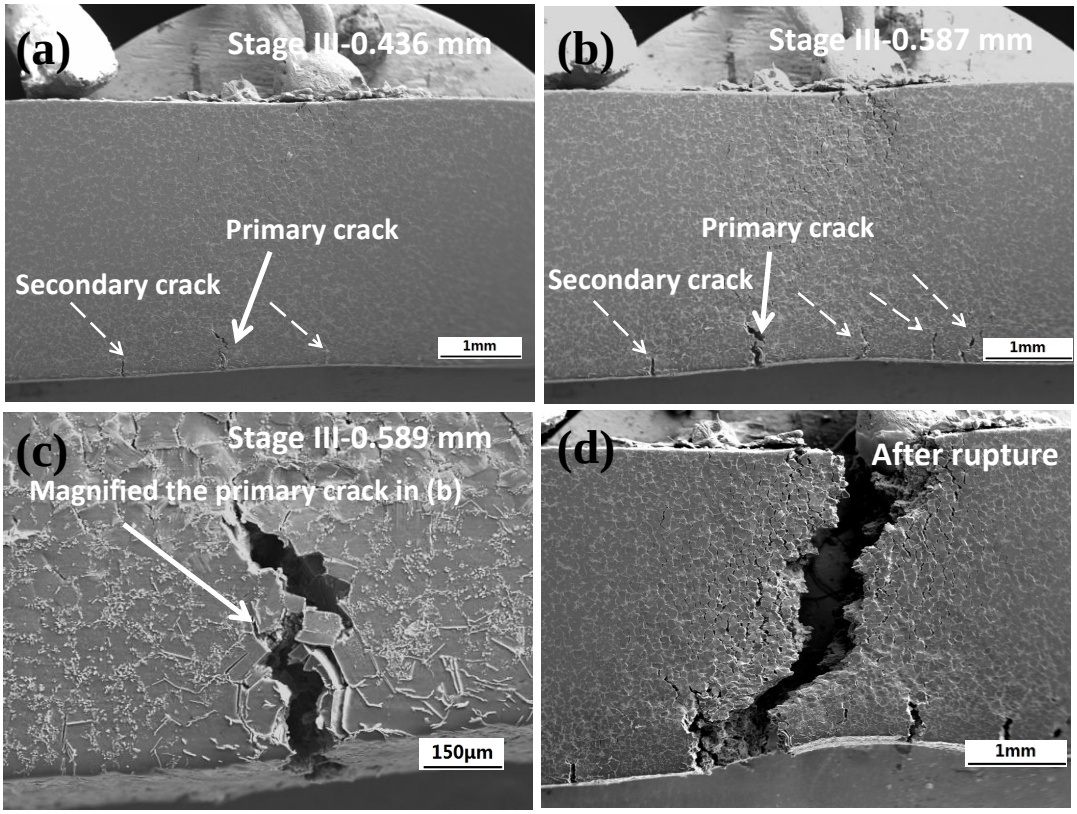

Fig. 24. Secondary electron SEM photomicrographs taken during an *in-situ* creep test at T=573K and σ=50MPa illustrating edge cracking initiation and propagation. The creep stages and displacements were indicated in the figures. The tensile axis was horizontal.

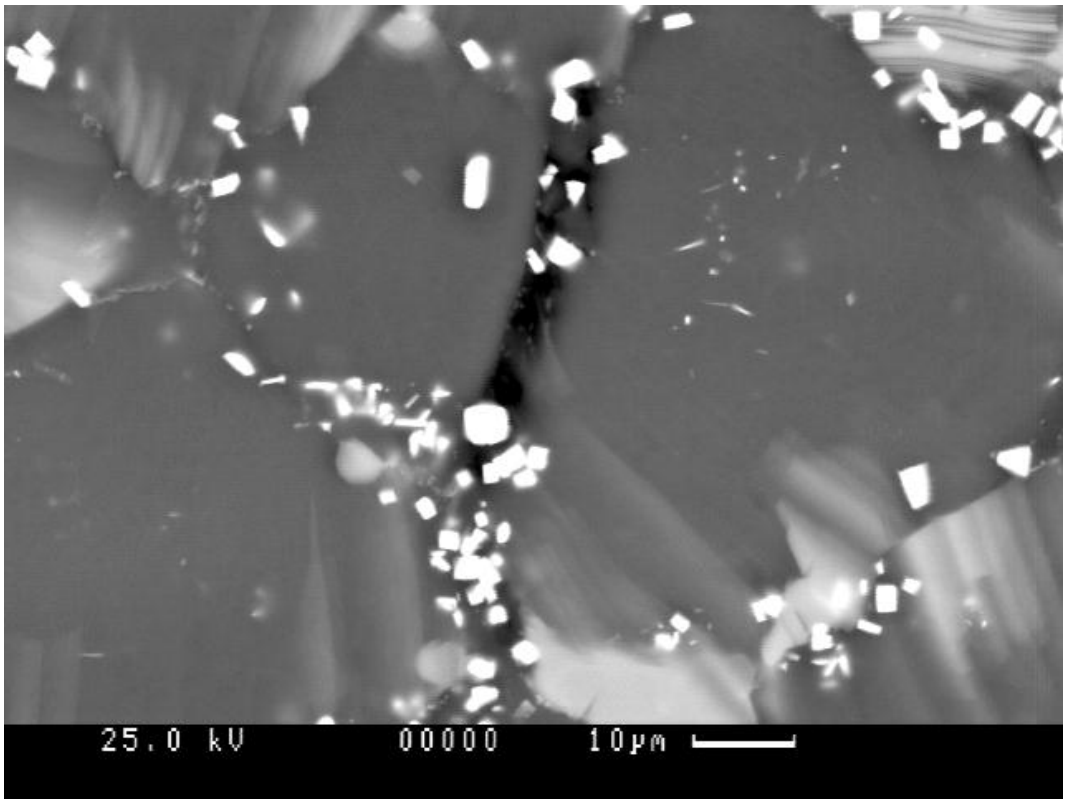

Fig. 25. Backscatter electron SEM photomicrograph represents a grain boundary cracking in the subsurface bulk microstructure of an *in-situ* creep tested specimen at T=573K and σ=50MPa.